NMR and birefringence study of structural transitions in disordered crystals: $Rb_xK_{1-x}MnF_3$

F. Borsa*

*Ames Laboratory–U.S. ERDA and Department of Physics,[†] Iowa State University, Ames, Iowa
and Istituto di Fisica dell'Università, Pavia, Italy*

D. J. Benard and W. C. Walker

Department of Physics,[‡] University of California, Santa Barbara, California

A. Baviera

Istituto di Fisica dell'Università and Unità di Pavia del Gruppo Nazionale di Struttura della Materia, Pavia, Italy

Measurements of ^{39}K and ^{87}Rb NMR and of modulated birefringence have been performed in $Rb_xK_{1-x}MnF_3$ mixed single crystals ($x = 0.02$, 0.04, 0.06, 0.1, 0.15, 0.27) in the temperature range 60–300 K. It was found that the structural phase transition which occurs at 184 K in pure $KMnF_3$ is moved towards lower temperatures upon substitution of K with Rb. The approximate law valid for x up to 0.15 is $T_c(x) = T_c(0)(1 - 2x) \simeq T_c(0)(1 - x)^2$. The result is discussed in terms of the cation effect on the stability of the cubic perovskite structure. The rotation angle φ of the MnF_6 octahedra appears to remain the order parameter with the average rotation angle decreasing as x increases. The NMR results indicate in addition that for $x \geq 0.02$, φ becomes nonuniform over distances of a few lattice spacings. A distribution of φ having a rms width of about 7.5% of the average φ is found for the sample $x = 0.02$. The birefringence results indicate that the first-order discontinuity at T_c is still present for $x = 0.02$ and 0.04 but is rounded off for $x \geq 0.06$. This result is interpreted in terms of a spatial distribution of transition temperatures due to the statistical fluctuations in concentration within "correlation volumes."

I. INTRODUCTION

Structural phase transitions in perovskite-type crystals of general formula ABO_3 have attracted a great deal of interest in recent years.[1-3] In many of these compounds, of which $SrTiO_3$ is one of the most investigated, there exists a cubic to tetragonal, purely structural (i.e., nonferroelectric) phase transition of second order or weakly first order whose order parameter is represented by the angle of rotation of the BO_6 octahedra around one of the axes of the original cubic cell. These transitions display many "universal" features common to other phase transitions, such as liquid-gas and magnetic phase transitions, both in the dynamical and static properties including a behavior described by nonclassical critical exponents near T_c.[4] Theoretically, it has been shown[5] that a simple model Hamiltonian, expressed in terms of local effective coordinates which describe the rotation of the BO_6 octahedra and the short-range interactions among the octahedra, is quite successful in explaining the experimental results.

$KMnF_3$ is a crystal of the type described above, displaying a weak first-order cubic to tetragonal phase transition at about 184 K.[6] On the other hand the isomorphous crystal $RbMnF_3$ remains cubic to very low temperatures. Together they form mixed crystals, $Rb_xK_{1-x}MnF_3$, over the whole concentration range which retain the cubic perovskite structure at high temperature. Since the cation seems to have a very important role in stabilizing the cubic structure, one expects that the substitution of K with Rb should change the local potential well in which the MnF_6 octahedra move and/or the interaction between adjacent octahedra. This should result in a randomization of the system with a corresponding reduction of the correlation effects between MnF_6 octahedra which remain, however, the basic units of the phase transition. The similarity of such a system with a disordered paramagnet obtained by diluting the magnetic ions with a diamagnetic species is suggestive. The purpose of the present work is to investigate the structural phase transition in $Rb_xK_{1-x}MnF_3$ mixed crystals as a function of Rb concentration. This includes the effect of Rb substitution on the transition temperature, the effect on the weak first-order discontinuity of the order parameter and on the value and temperature dependence of the order parameter itself. It should be noted that a considerable amount of work has been done in disordered structures known as dirty displacive ferroelectrics.[7] However, the long-range character of the dipolar forces present in ferroelectrics and the first-order character of the structural transitions make the problem involved in the study of dirty displacive ferroelec-

trics quite different from the one which is investigated here even though common traits can certainly be found.

Both modulated birefringence[8] and NMR[9] techniques have been employed successfully by the present authors in the study of the structural phase transition in pure $KMnF_3$. The combined use of both these techniques seem to be very well suited to the investigation of the mixed crystals. In fact the birefringence measures the average structural distortion over a macroscopic domain while the NMR measures the local distortion of the lattice cell and is, therefore, sensitive to any nonuniformity of the distortion over distances of a few lattice spacings.

II. EXPERIMENTAL

A. NMR measurements

The measurements of ^{39}K and ^{87}Rb NMR were performed with a Varian wide-line spectrometer and a continuous averaging technique as described previously.[9]

The total shift of the ^{39}K (or ^{87}Rb) NMR line in the presence of second-order quadrupole effects can be written[10]

$$\frac{\Delta H}{H} \simeq \frac{\Delta \nu}{\nu_L} = \left(\frac{\Delta \nu}{\nu_L}\right)_M - \frac{3\nu_Q^2}{16\nu_L^2}(1 - \mu^2)(9\mu^2 - 1) \ , \tag{2.1}$$

where ν_L is the Larmor frequency, ν_Q is the quadrupole coupling frequency, and $\mu = \cos\theta$ with θ the angle formed by the directions of $\vec{H}$ and the axis of axial symmetry $\vec{c}$ of the crystal in the low-temperature phase. In pure $KMnF_3$ and above T_c the crystal is cubic ($\nu_Q = 0$) and the shift $\Delta H/H$ is determined by the hyperfine interaction of the nucleus with the paramagnetic manganese ions, i.e., $(\Delta\nu/\nu_L)_M$. Below T_c the point symmetry at the potassium site becomes tetragonal and the nucleus experiences an axially symmetric electric field gradient. It was found in the previous work[9] that in a single crystal oriented with $\vec{H} \parallel [100]$ one can detect two resonance lines below T_c. One line originates from domains with $\vec{c} \parallel \vec{H}$ and the other originates from domains with $\vec{c} \perp \vec{H}$ with a relative intensity of 1:2, respectively. Since the anisotropy of the magnetic shift is negligible at all temperatures one can safely assume that the distance between the two signals observed below T_c is a direct measure of the strength of the quadrupole interaction according to the equation

$$\left(\frac{\Delta\nu}{\nu_L}\right)_{\vec{H} \perp \vec{c}} - \left(\frac{\Delta\nu}{\nu_L}\right)_{\vec{H} \parallel \vec{c}} = \frac{3}{16}\frac{\nu_Q^2}{\nu_L^2} \ , \tag{2.2}$$

where, for $I = \frac{3}{2}$, $\nu_Q = \frac{1}{2}e^2qQ/h$ with q being the largest component of the electric field gradient (EFG) tensor and Q being the nuclear quadrupole moment. Furthermore, we know from measurements in pure $KMnF_3$ that $\nu_Q \propto \varphi^2$, where φ is the rotation angle of the MnF_6 octahedra below T_c and is the order parameter for the structural phase transition in these perovskite-type crystals.

If the symmetry of the EFG is not axial then the second-order quadrupole shift given by Eq. (2.1) should be modified to include the dependence upon the asymmetry parameter $\eta = (V_{xx} - V_{yy})/V_{zz}$ and the azimuthal angle of the magnetic field H in the xy plane, where x, y, z are the principal axes of EFG tensor and z is the direction of the largest component. As will be seen in the following discussion a situation can arise in which the local EFG lacks axial symmetry if the rotation angle φ is not uniform over distances of a few lattice spacings. In such a case one expects that the average quadrupole shift given by Eq. (2.2) should be corrected by introducing a numerical factor, smaller than unity, which takes into account the average effect of the local deviation from axial symmetry.

The shift of the center of the resonance line is obtained by measuring the resonance field and assuming for the gyromagnetic ratios the values $\gamma = 198.7$ for ^{39}K and $\gamma = 1393.2$ for ^{87}Rb. The measurements were performed on samples of ellipsoidal shape, with $\vec{H}$ oriented along one of the [100] directions. The experimental shifts were not corrected for the effect of the demagnetizing field. The temperature was varied with a standard nitrogen gas-flow system providing a long-term stability of about 0.5 °K and a temperature variation over the size of the sample of the same order of magnitude. The quadrupole line broadening below T_c owing to the temperature gradients over the sample was estimated and found to be negligible even in the temperature interval where the temperature dependence of ν_Q is greatest.

B. Birefringence measurements

The measurement of birefringence was accomplished by use of a polarization-modulated He-Ne-laser source and synchronous detection.[8] When a $Rb_xK_{1-x}MnF_3$ sample of length l, with static birefringence δn, and an oscillating wave plate are placed in series between crossed polarizers, a monochromatic beam of light of wave vector k will pass normally through the over-all optical train with a time varying transmission T of the form

$$T(t) = T_{dc} + T_{ac} [J_1(\phi) \sin\omega t \sin kl\delta n$$
$$+ J_2(\phi) \sin2\omega t \cos kl\delta n + \cdots] \ ,$$

where ω is the frequency and ϕ is the amplitude of oscillation of the wave plate. Therefore, one can obtain a measurement of the birefringence on the static sample by taking the ratio of the intensities of the fundamental and second-harmonic components of the transmission:

$$\delta n = \frac{1}{kl} \frac{J_1(\phi)}{J_2(\phi)} \tan^{-1}\left(\frac{T(\omega)}{T(2\omega)}\right) .$$

The source of monochromatic light was a 2-mW He-Ne laser internally polarized by a Brewster-angle plate. The output of the laser was directed through a Morvue polarization modulator which served as an oscillating wave plate, excited at 50 kHz by an attached piezoelectric transducer. The sample was held on a copper plug mounted on a cold finger inside a sealed chamber that was evacuated to 10^{-6} Torr by sorption roughing and a sustaining ion pump. Upon exiting the vacuum housing the beam was intercepted by an analyzing polaroid filter and an end-on photomultiplier tube. The electrical output of the photomultiplier tube was amplified and analyzed electronically by synchronous detectors at 50 and 100 kHz. Phase references were obtained from the 50-kHz oscillator, which was used to excite the acoustically driven wave plate. The ratio of the 50- to 100-kHz signal intensities was obtained from an analog-divider integrated circuit and then chart recorded versus the temperature of the sample.

In order to compensate for any birefringence in the windows of the vacuum chamber an additional static quarter wave plate was mounted between the oscillating wave plate and the entrance window. This made it possible to zero out any small extraneous birefringence by rotating the quarter wave plate to yield zero transmission of the fundamental modulation component at room temperature, where the sample is known to have cubic symmetry and hence zero birefringence. It was also possible to calibrate the sensitivity of the instrument with rotation of the wave plate by adjusting it to yield the conditions $kl\delta n = 0$ where $T(2\omega) = T_{ac}J_2(\phi)$ and alternately $kl\delta n = \frac{1}{2}\pi$ where $T(2\omega) = 0$ and $T(\omega) = T_{ac}J_1(\phi)$.

The sample temperature was obtained by measuring the voltage across a Pt wire resistor (2000 Ω at 300 °K) which was embedded in the cold finger and attached to a precision 1-mA current source and a field-effect-transistor input precision voltage follower by a four-wire cable.

The sample temperature was then swept by admitting liquid nitrogen to the cold-finger Dewar, which was initially held at room temperature. The thermal coupling between the Dewar and cold finger was variable by means of an adjustable thermal impedance. The negative thermal slewing rate of the sample in these experiments was on the order of ~50 mK/sec. The lowest temperature reached (~60 °K) were obtained by pumping on liquid oxygen. After cooling to well below T_c the samples, birefringence was also measured as the temperature was allowed to rise at a rate of ~10 mK/sec to room temperature. The rate of temperature rise could be accelerated to ~50 mK/sec by blowing compressed air into the Dewar after boiling out excess liquified gas. By observation of the sharpness of the changes in birefringence and any shifts in T_c between positive and negative thermal sweeps as well as at varying slew rates, it was possible to assess the effect of any thermal lags between the sample and the cold finger or any hysteresis that may occur in the temperature dependence of the sample's birefringence. These data and previous work in which the 186 K phase transition in pure KMnF$_3$ was studied, showed that the instrumental resolution on the slower sweeps was not limited by their response time of the electronic analysis or the thermal equilibration of the sample, but rather by the spatial variation of the sample across the probing laser beam. By aperturing the laser beam with a 100-μm pinhole placed immediately before the sample, this effect was eliminated giving a resolution of ~20 mK. In this study, however, somewhat larger pinholes and thermal slewing rates were employed, thus limiting resolution to ~50 mK, which was, however, adequate for the determination of T_c and the observation of non-classical effects in the temperature dependence of δn near T_c. Under these conditions the thermal lag between the sample at the point being probed and the Pt wire resistor was negligible compared to the resolution limit on the slow upward sweeps of the sample temperature.

C. Crystal growth

The pure crystals of KMnF$_3$ and RbMnF$_3$ were prepared by reacting either analytical-reagent grade KF or RbF with MnCO$_3$ in a 20 volume % HF acid solution. The dried precipitate was then crystallized under a stream of dry HF by the standard Bridgeman-Stockbarger technique at a rate of 4–5 mm/h. The stoichiometric portions of the resulting boules were then separated out and used as the starting materials for the synthesis of the mixed Rb$_x$K$_{1-x}$MnF$_3$ crystals.

The desired proportions of the stoichiometric KMnF$_3$ and RbMnF$_3$ crystals were ground, weighed, mixed, and similarly recrystallized at a rate of 2 mm/h and then annealed at 950 ± 25 °C for 16 h prior to slowly cooling to room temperature at a rate of ~100 °C/h. No attempt was made to analyze

the relative K-Rb concentration in the melt; how-
ever, the consistency of the experimental results
indicated that the relative Rb concentrations among
the various samples was preserved.

The samples thus produced were ground to the
ellipsoidal shape appropriate for the NMR experi-
ments and examined in white light between crossed
polaroids for any sign of noncrystalline structure,
lack of optical homogeneity, or phase separation
into regions of differing stoichiometry. None
were detected in any of the samples used.

The preparation of the birefringence samples,
which were polished plates of dimensions (0.5 cm
× 0.5 cm × 0.1 mm) oriented along [100] crystal-
line axes, was then made from the same crystals
used in the NMR experiments. After a crystal
was oriented by x rays, the birefringence sample
was cleaved from it and then ground to the desired
thickness. A high optical polish was applied to
both faces of the platelet by an automatic polishing
wheel with a diamond-embedded polishing cloth
surface. The finished birefringence samples were
also reexamined between crossed polaroids in
white light for any signs of nonuniformity and, if
satisfactory, were then mounted to the copper
plug by a small drop of epoxy applied at the end
of the sample furthest from the point on the sur-
face to be probed in the birefringence experiment.

III. RESULTS

A. Birefringence

The birefringence of the $Rb_xK_{1-x}MnF_3$ samples
with varying compositions, $x = 0, 2, 4, 6, 10, 15, 27$
at.%, was measured to determine accurately the
shift in T_c that occurs and to note any changes
that may take place in order or rounding of the
structural phase transition in the critical region
near T_c. Pure $KMnF_3$ was studied previously by
this technique. The 184 °K transition was shown
to be first order by the discontinuity in δn (~1.38
$\times 10^{-4}$) which occurs at T_c.[8] Above T_c the bire-
fringence was zero, and below T_c the birefrin-
gence was fit to a power law with a $\frac{2}{3}$ exponent
and an "effective T_c" displaced 1.7 °C above the
actual temperature of the phase transition. In
order to determine this effective value of T_c it
was necessary to measure the slope of the bire-
fringence versus temperature at T_c, which was
found to be $(\partial \delta n/\partial T)_{T=T_c} \approx 5.4 \times 10^{-5}/°C$. Upon
substitution of Rb for K atoms in the crystalline
samples there were noted several systematical
changes in the features of the birefringence sig-
nature near T_c, which include (i) a depression
of T_c with increasing x, (ii) progressive rounding
of the transition, and (iii) a decrease in the slope
$\partial \delta n/\partial T$ below T_c. These effects are shown in
Fig. 1 which depicts the birefringence near T_c for
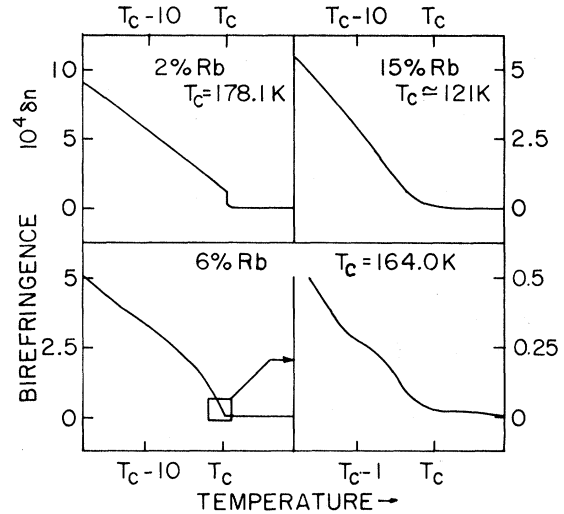
FIG. 1. Plot of the birefringence as a function of tem-
perature for three representative samples of
$Rb_xK_{1-x}MnF_3$ with $x = 0.02$, 0.06, 0.15. The region close
to T_c is shown on a enlarged scale for $x = 0.06$.

samples with $x = 2$, 6, and 15 at.%. Up to $x = 4$ at.%
the only noticeable effect on the phase transition
was a lowering of T_c at the rate $\partial T_c/\partial x = -360$ °C.
The magnitude of the discontinuity and the slope
of birefringence at T_c were basically unchanged,
although at $x = 4$ at.% it was found that $(\partial \delta n/\partial T)_{x=0.04}$
$\sim 0.7(\partial \delta n/\partial T)_{x=0}$. Thus up to $x = 0.04$ the transition
remains first order. At $x = 0.06$ the first-order
discontinuity disappears and δn is continuous at
T_c and approaches T_c from below linearly with a
slope of $\sim 5 \times 10^{-5}/°C$; however, approximately
3 °C below $T_c = 164$ °K a second slope change occurs
reducing the slope by a factor of roughly 2, as
shown in the figure. Further, upon close exam-
ination of the birefringence near T_c, as shown in
the enlargement, there is the beginning of a high-
temperature tail in the birefringence above T_c.
The tail extends ~800 mK above T_c and is of mag-
nitude 2.5×10^{-6} at T_c. Upon further increases in
the Rb content x, the transition is progressively
rounded to even higher order. For $x = 15$ at.%
both δn and $\partial \delta n/\partial T$ are continuous at T_c. The high-
temperature tail is strongly developed and it be-
comes difficult to assign a definite value for T_c.
The slope of the birefringence in this case, how-
ever, does not decline further. The remaining
sample with $x = 27$ at.% showed no evidence of
any structural rearrangement within the limit of
instrumental sensitivity, $\delta n \sim 10^{-7}$, down to the
lowest available temperature ~60 °K.

B. ^{39}K nuclear magnetic resonance

The results obtained for the ^{39}K NMR in
$KMnF_3 : 2$-at.% Rb are shown in Fig. 2(a). From
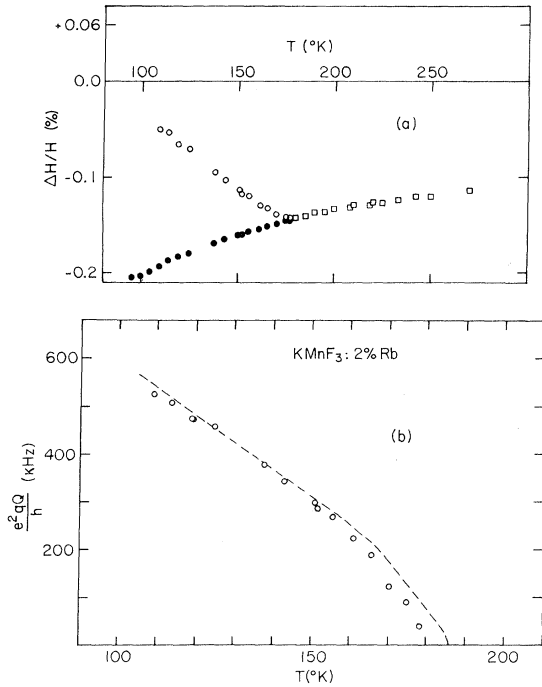
FIG. 2. (a) Shift of the ^{39}K NMR line in KMnF$_3$: 2-at.% Rb as a function of temperature measured at 3 MHz. The resonance line splits below T_c in two lines corresponding to domains with $\vec{H} \| \vec{c}$ (solid circles) and to domains with $\vec{H} \perp \vec{c}$ (open circles). (b) Temperature dependence of the ^{39}K quadrupole coupling constant. The dashed curve represents the behavior of the QCC in pure KMnF$_3$.

the splitting of the line due to the quadrupole interaction one can infer the value of the transition temperature, $T_c = 179 \pm 2$ K, which is lower than the value obtained in pure KMnF$_3$, $T_c = 186 \pm 1$ K. By making use of relation (2.2) and the experimental shifts one can extract the values of the quadrupole coupling constant (QCC). These are plotted in Fig. 2(b) and compared with the corresponding values for pure KMnF$_3$. A quantitative analysis of the data in terms of critical exponents for the temperature dependence of the order parameter is not warranted in view of the experimental uncertainty near T_c owing to the broadening of the signal discussed below. Qualitatively the temperature behavior of the QCC and consequently of the rotation angle φ, seems to be approximately the same as in KMnF$_3$ including the nonclassical critical effects.[11]

The ^{39}K linewidth in the 2-at.% Rb sample is more indicative of a different behavior with respect to pure KMnF$_3$. The results are shown in Fig. 3. By comparison one notes that the line broadening observed below T_c in pure KMnF$_3$, not shown in the figure which is for both $\vec{H} \| \vec{c}$ and

$\vec{H} \perp \vec{c}$ is on the order of the broadening reported in Fig. 3 for $\vec{H} \| \vec{c}$. There are no second-order quadrupole effects in this orientation as per Eq. (2.1). Furthermore, the broadening of the line with $\vec{H} \perp \vec{c}$ in the 2-at.% Rb sample is inversely proportional to the resonance frequency indicating an inhomogeneous quadrupole broadening. These observations lead us to conclude that in the 2-at.% Rb sample the distortion from cubic symmetry below T_c is associated with a rotation angle that varies locally in space.

Measurements of the ^{39}K paramagnetic shift were performed in a number of crystals of different concentration of Rb and the results are shown in Fig. 4. For concentrations of Rb above 2 at.% the line broadening of the resonance for $\vec{H} \perp \vec{c}$ becomes so severe, below T_c, that it is not possible to follow its shift as a function of temperature. The transition temperatures T_c indicated in Fig. 4 were obtained by plotting the relative peak intensity of the signal as a function of temperature. As shown in Fig. 5 for the 6-at.% Rb sample, the signal intensity decreases abruptly starting at $T \simeq T_c$ owing to the rapid broadening and shifting away of the signal which results from the domains having $\vec{H} \perp \vec{c}$, while an additional decreasing of the peak amplitudes of the signal comes from broadening of the $\vec{H} \| \vec{c}$ resonance itself. The values for the transition temperatures obtained from the analysis of the signal intensity are

$$T_c = \begin{cases} 171 \pm 2 \text{ K for 4 at.\%,} \\ 160 \pm 2 \text{ K for 6 at.\%,} \\ 150 \pm 2 \text{ K for 10 at.\%,} \\ 143 \pm 5 \text{ K for 15 at.\%.} \end{cases}$$
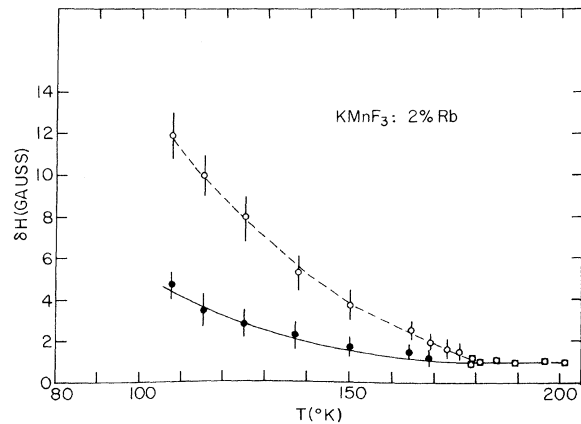
FIG. 3. Peak-to-peak derivative linewidth of the ^{39}K NMR line as a function of temperature at 3 MHz. (●) Resonance from domains with $\vec{H} \| \vec{c}$. (○) Resonance from domains with $\vec{H} \perp \vec{c}$. The solid and dashed lines are an aid to the eye.
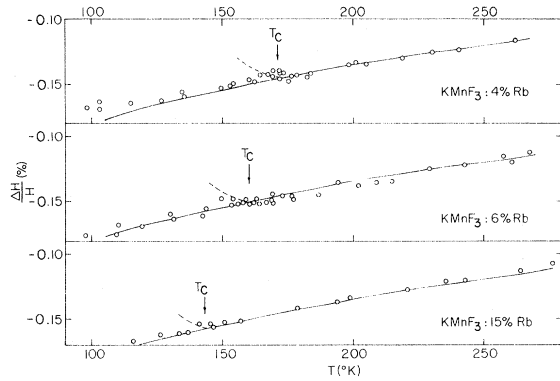
FIG. 4. Shift of the ^{39}K NMR line as a function of temperature at 3 MHz for samples with different atomic concentrations of Rb. The temperature at which the structural transition is thought to occur is indicated by an arrow. The resonance from domains with $\vec{H} \perp \vec{c}$, suggested by the dashed line, becomes too broad to be measured. The solid curves are a fit of the paramagnetic shift according to a Curie-Weiss law $\Delta H/H$ (%) $= -54(T+200)^{-1}$. The fact that the same curve fits the data for different samples shows that the magnetic properties are not appreciably modified by the Rb substitution.

A preliminary conclusion is that the structural phase transition seems to be well defined up to 15-at.% Rb concentration, but the order parameter φ appears to be spatially nonuniform. A more quantitative discussion on this point is presented in Sec. IV.

C. ^{87}Rb nuclear magnetic resonance

The study of the quadrupole effects at the rubidium site should, in principle, allow one to obtain
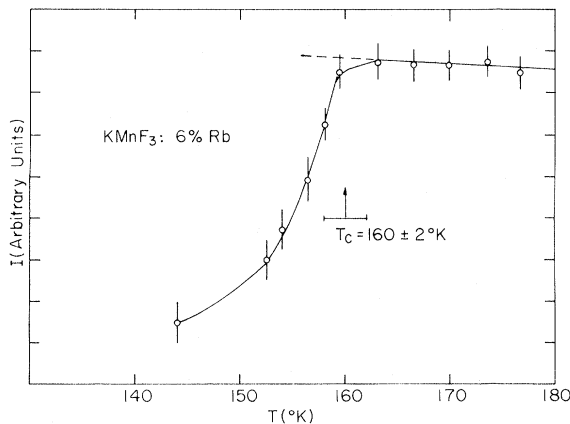
FIG. 5. Peak-to-peak derivative signal intensity of ^{39}K NMR as a function of temperature at 3 MHz. The solid and dashed curves are only an aid to the eye.

additional information about the structural phase transition in these mixed crystals. However, in practice we found this study difficult. In fact if one chooses to work at the same resonance frequency as for ^{39}K (2-4 MHz) one finds that the sensitivity for both the ^{85}Rb and ^{87}Rb NMR is too low. At higher resonance frequencies the measurements are feasible but the second-order quadrupole effects are small since the quadrupole shift goes as ν_L^{-2} [see Eq. (2.2)]. Some typical measurements of ^{87}Rb NMR are shown in Fig. 6 for two concentrations of rubidium. The structural phase transition occurs at 160 °K for 6-at.% Rb and at 150 °K for 10-at.% Rb as it can be deduced from the ^{39}K NMR and from the birefringence measurements. However, as it can be seen from the NMR-shift measurements of Fig. 6, it is only below 100 K that measurable quadrupole effects appear. The ^{87}Rb resonance arising from the domains with $\vec{H} \perp \vec{c}$ resonance are indicated by the solid circles and squares in Fig. 6. A rough estimate of the quadrupole coupling frequency ν_Q extrapolated at zero temperature yields

$$\nu_Q(0) \sim 1.3 \text{ MHz for } ^{87}\text{Rb in } KMnF_3 : 6\text{-at.}\% \text{ Rb,}$$

$$\nu_Q(0) \sim 0.9 \text{ MHz for } ^{87}\text{Rb in } KMnF_3 : 10\text{-at.}\% \text{ Rb.}$$

$$(3.1)$$

Since $\nu_Q(T) \propto \varphi^2(T)$,[9,11] the expression $\nu_Q(T)$ $= \nu_Q(0)[(T_c - T)/T_c]$ was used to extrapolate to $T = 0$ along with the value of $\nu_Q(T)$ which can be deduced from Eq. (2.2) and the measured splitting at about $T = 100$ °K obtained from the data in Fig. 6. Because of the large experimental uncertainty in the
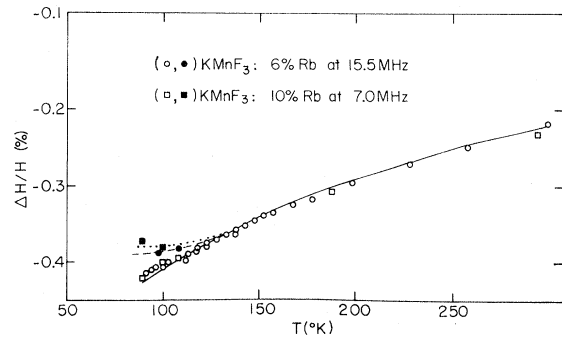
FIG. 6. Shift of the ^{87}Rb NMR line as a function of temperature. The solid curve is a fit of the paramagnetic shift according to the Curie-Weiss law $\Delta H/H$ (%) $= -97(T+135)^{-1}$. ($\bullet$, $\blacksquare$) Domains with $\vec{H} \perp \vec{c}$. (O, □) Domains with $\vec{H} \parallel \vec{c}$. The dashed curve refers to 6-at.% Rb and corresponds to the behavior predicted by Eq. (2.2) for the quadrupole splitting with $\nu_Q = 1.3[(160 - T)/160]$ MHz. The dotted curve is the same for $\nu_Q = 0.875[(150 - T)/150]$ MHz and it refers to 10-at.% Rb.

measurement of the quadrupole shift and of the fact that Eq. (2.2) is valid only for an axially symmetric EFG's, the results quoted have to be viewed only as indicative.

The QCC of ^{87}Rb can be compared to the QCC of ^{39}K obtained by extrapolating the data of Fig. 2 to zero temperature. We obtain

$$\nu_Q(0) = 583 \pm 10 \text{ kHz for } {}^{39}\text{K in KMnF}_3,$$

$$\nu_Q(0) = 567 \pm 10 \text{ kHz for } {}^{39}\text{K in KMnF}_3 : 2\text{-at.\% Rb}.$$

$$(3.2)$$

Unfortunately no measurements of QCC at both the ^{39}K and ^{87}Rb site were possible in the same crystal. By scaling the values of $\nu_Q(0)$ for ^{87}Rb by the ratio of the quadrupole moments $Q\,(^{87}\text{Rb})/Q(^{39}\text{K}) = 2$ and by the ratio of the antishielding factors $(1 - \gamma_\infty)_{\text{Rb}}/(1 - \gamma_\infty)_{\text{K}} = 3$ one finds that the estimated quadrupole coupling constant should be

$$\nu_Q(0) \sim 200 \text{ kHz for } {}^{39}\text{K in KMnF}_3 : 6\text{-at.\% Rb},$$

$$\nu_Q(0) \sim 150 \text{ kHz for } {}^{39}\text{K in KMnF}_3 : 10\text{-at.\% Rb}.$$

$$(3.3)$$

These values are considerably smaller than the values measured directly in pure KMnF$_3$ and KMnF$_3$: 2-at.% Rb from the ^{39}K NMR. This could indicate either that the average angle of distortion of the low-temperature phase falls off rapidly with increasing ^{87}Rb content or that the average local distortion as probed by ^{87}Rb nuclei is smaller than the one probed by ^{39}K nuclei. Also it should be noted that if the order parameter is nonuniform over distances comparable to a lattice spacing then the local symmetry can be different from axial. Then the right-hand side of Eq. (2.2) should be multiplied by a factor less than unity, as discussed previously, and hence the estimate QCC would be greater.

IV. INTERPRETATION AND DISCUSSION OF THE EXPERIMENTAL RESULTS

A. Concentration dependence of the transition temperature

The temperature T_c of the transition from the cubic high-temperature perovskite structure to the tetragonal phase is plotted in Fig. 7 as a function of rubidium concentration x. The agreement between the NMR and birefringence results is very good with the exception of 15-at.% Rb concentration. A possible explanation for the discrepancy is that the decrease in the NMR signal determines the temperature at which short-range order develops, where we mean by short-range order the formation of locally distorted regions in the sample, while the birefringence measures
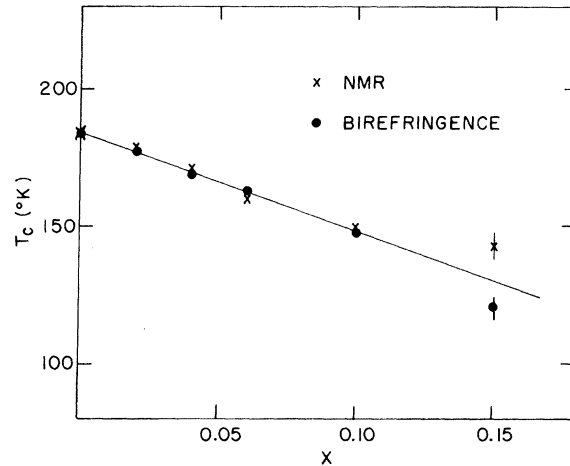
FIG. 7. Transition temperature of the structural phase transition in Rb$_x$K$_{1-x}$MnF$_3$ as a function of rubidium concentration.

the onset of true "long-range order." This interpretation is corroborated by the presence of a tail in the birefringence above T_c as shown in Fig. 1, which may be due to short-range order. Furthermore, a sample containing 27-at.% Rb failed to show any structural transition down to 60 °K indicating that the deviation from the straight line in Fig. 7 is towards lower values of T_c in agreement with the birefringence measurements rather than towards higher values of T_c as one would infer from the NMR point at 15-at.% Rb. In any case, both sets of results yield a concentration dependence of T_c described approximately by the law

$$T_c(x) = T_c(0)(1 - 2x) \simeq T_c(0)(1 - x)^2.$$

The decrease of T_c with increasing Rb concentration is qualitatively in accord with the fact that pure RbMnF$_3$ remains cubic at any temperature. The stability of the cubic perovskite structure in the AMnF$_3$ compounds (A = Li, Na, K, Rb, Cs) is understood in terms of the empirical Goldschmidt rule.[12] To illustrate this we have represented in Fig. 8 the cubic perovskite structure as a framework of MnF$_6$ octahedra sharing corners, with the cation ion occupying the cavity within the MnF$_6$ octahedra. The size of the cavity is determined by $a = 2(r_{\text{Mn}} + r_{\text{F}})$ where r is the ionic radius for the Mn^{2+} and F$^-$ ions. According to Goldschmidt's rule the structure is stable if the cavity is completely filled, namely, if the ratio

$$t = 1.1\,(r_A + r_F)/\sqrt{2}\,(r_{\text{Mn}} + r_{\text{F}}) \tag{4.1}$$

is close to 1. The coefficient 1.1 has been introduced to correct for 12-coordination. The values given in Table I show that only RbMnF$_3$ and KMnF$_3$
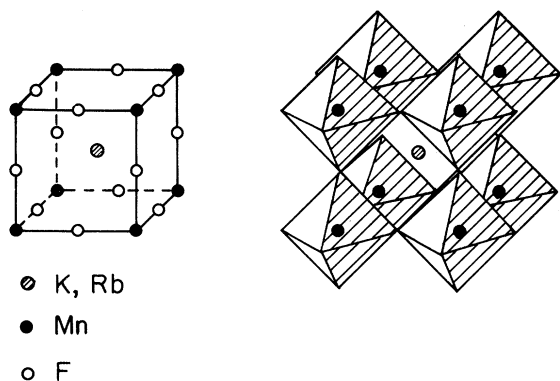
FIG. 8. Cubic perovskite structure of $KMnF_3$.

⊘ K, Rb

● Mn

○ F

have values of t close to 1, in agreement with the fact that only these two compounds possess the cubic perovskite structure at room temperature. The distortion of $KMnF_3$ at lower temperature is consistent with the fact that the K^+ ions are slightly too small to fill the cavity.

Since the Goldschmidt approach is based essentially on the cation-size effect it is instructive to make a comparison between our results and a recent study of the pressure dependence of T_c in pure $KMnF_3$.[13] Okai and Yoshimoto find a linear dependence of T_c from pressure up to 10 kbar with $dT_c/dp = 3.9\,°K/kbar$. Using the value for the compressibility of $RbMnF_3$, i.e., $K = (1/V)(dv/dp)$ $= -14.8 \times 10^{-4}\,kbar^{-1}$, one can calculate the volume dependence of T_c from the pressure dependence which yields $V\,dT_c/dV \simeq -0.26 \times 10^4\,°K$, i.e., $0.26\,°K$ for a 10^{-4} fractional change in volume. On the other hand from the linear concentration dependence of T_c shown in Fig. 7 one obtains $dT_c/dx = -360\,°K$. Then by use of the known lattice parameters $a = 4.191\,Å$ for $KMnF_3$ and $a = 4.234\,Å$ for $RbMnF_3$ and by assuming a linear interpolation for the mixed crystals, we determine the average volume change as a function of Rb concentration as

$$\frac{1}{V}\frac{dV}{dx} \simeq \frac{3}{a}\frac{da}{dx} = 3.07 \times 10^{-2}.$$

The concentration dependence of T_c can now be converted into a volume dependence giving $V\,dT_c/dV \simeq -1.2 \times 10^4\,°K$. This calculated value based

on our results has the same sign but is considerably larger than the value obtained from the pressure dependence of T_c. The disagreement in the order of magnitude indicates that the effect on T_c due to the introduction of Rb atoms in $KMnF_3$ is not a simple effect owing to the average volume expansion produced in the lattice by the larger Rb atom.

The dependence of T_c on Rb concentration is reminiscent of the observed decrease of the magnetic transition temperature upon dilution of the magnetic ion. A linear dependence of the transition temperature on concentration is obtained theoretically from a molecular-field-approximation treatment of the disordered Heisenberg model when the nearest-neighbor exchange interaction between magnetic ions is assumed to be independent of concentration.[14] The experimental results shown in Fig. 7 seem to indicate, instead, a quadratic temperature dependence of T_c upon the potassium concentration $(1 - x)$. For structural phase transitions Thomas[5] has developed a model Hamiltonian in terms of local coordinates describing the MnF_6 octahedra rotation, which is quite successful in predicting the main features of the structural phase transitions in the molecular-field approximation. It is conceivable that this model Hamiltonian can be applied to treat a disordered system such as $Rb_xK_{1-x}MnF_3$.

B. Spatial variation of the order parameter

The qualitative picture for the structural transitions in disordered $Rb_xK_{1-x}MnF_3$ crystals as it emerges from the NMR and birefringence results is the following. On the average, in each macroscopic domain the symmetry of the low-temperature phase is the same as for $KMnF_3$ and there is a well-defined average order parameter. On the other hand within each domain the order parameter (i.e., the rotation angle of MnF_6 octahedra) appears to be spatially nonuniform.

A simplified quantitative analysis of the NMR data can be attempted for the crystal with $x = 0.02$. Assuming that the local distribution of the order parameter can be described by a Gaussian function,

TABLE I. Values of Goldschmidt's ratio (4.1) for $AMnF_3$ compounds. The following values for the ionic radii have been used: $r_{F^-} = 1.33\,Å$; $r_{Mn^{+2}} = 0.8\,Å$.

	$A = Li$ $(r = 0.78\,Å)$	$A = Na$ $(r = 0.98\,Å)$	$A = K$ $(r = 1.33\,Å)$	$A = Rb$ $(r = 1.49\,Å)$	$A = Cs$ $(r = 1.65\,Å)$
t	0.76	0.84	0.97	1.03	1.09

$$P(\varphi) = \frac{1}{(2\pi)^{1/2}\Delta} \exp\left(-\frac{(\varphi - \langle\phi\rangle_{\mathrm{av}})^2}{2\Delta^2}\right), \qquad (4.2)$$

where $\langle\phi\rangle_{\mathrm{av}}$ is the average rotation angle, Δ^2 is the second moment of the distribution, and $P(\varphi)$ is the probability function renormalized to unity. For small values of x one assumes that the rotation angle varies very little over distances of the order of a few lattice spacings. Then the local symmetry of the distorted phase at the K or Rb position will still be axial as in pure $KMnF_3$ and the quadrupole interaction ν_Q is proportional to the square of the local rotation angle φ. By using expression (2.2) for the quadrupolar shift K and the fact that $\nu_Q \propto \varphi^2$ one finds for the average shift

$$\bar{K} = \frac{3}{16}\frac{\langle\nu_Q^2\rangle_{\mathrm{av}}}{\nu_L^2} = A\int P(\varphi)\varphi^4 d\varphi \simeq A(\langle\varphi\rangle_{\mathrm{av}})^4 + \cdots ,$$

$$(4.3)$$

while the second moment of the NMR line due to the different value of the quadrupole interaction from cell to cell is given by

$$\frac{\langle\delta H_Q^2\rangle}{H^2} = \int P(\varphi)(K - \bar{K})^2 \simeq \left(4A(\langle\phi\rangle_{\mathrm{av}})^4 \frac{\Delta}{\langle\phi\rangle_{\mathrm{av}}}\right)^2 + \cdots ,$$

$$(4.4)$$

where A is a constant and where we neglect terms of higher order in $\Delta/\langle\phi\rangle_{\mathrm{av}}$ since $\Delta \ll \langle\phi\rangle_{\mathrm{av}}$. From Eqs. (4.3) and (4.4) and by assuming a Gaussian shape for the NMR quadrupolar broadening we obtain for the NMR linewidth due to the distribution of rotation angles:

$$\delta H_Q = (\langle\delta H_Q^2\rangle)^{1/2} = 4\bar{K}H\Delta/\langle\phi\rangle_{\mathrm{av}}, \qquad (4.5)$$

where H is the external magnetic field. The difference in linewidth between the resonance lines for $\vec{H}\|\vec{c}$ and $\vec{H}\perp\vec{c}$ (see Fig. 3) represents, in our view, the additional broadening due to the spatial variation of the order parameter. According to Eq. (4.5) this additional broadening should be proportional to the quadrupolar shift. The values of $\delta H_Q \equiv \delta H_\perp - \delta H_\|$ are plotted in Fig. 9 as a function of the quadrupolar shift (shown in Fig. 2) the temperature being the implicit parameter. From the linear behavior of δH_Q vs $\bar{K}H$ one obtains as an indication for the dispersion in the rotation angle $\Delta \simeq 0.075\langle\phi\rangle_{\mathrm{av}}$.

For larger concentrations of Rb atoms the dispersion in the rotation angle is probably greater and the local symmetry at the K or Rb site is no longer axial since the rotation angle can vary appreciably within a few lattice spacings. In fact it is reasonable to think that the variation of the rotation angle should occur over a distance of the order of the average distance between Rb impurity atoms. The distance is of the order of four lattice
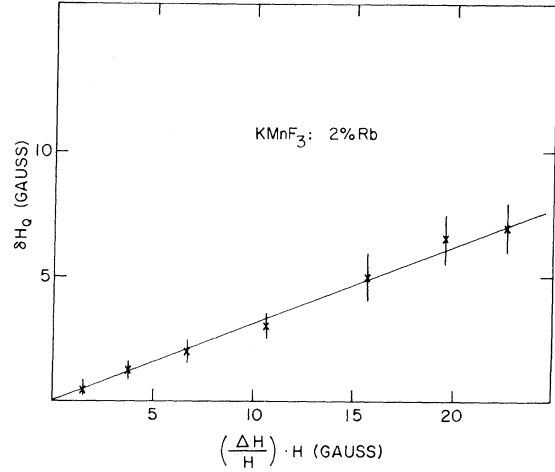
FIG. 9. Difference δH_Q between the broadening of the ^{39}K NMR line with $\vec{H}\|\vec{c}$ and with $\vec{H}\perp\vec{c}$ plotted as a function of the shift due to quadrupole interactions with the temperature as implicit parameter.

spacings for $x = 0.02$ and two lattice spacing for $x = 0.15$. One should keep in mind that the quadrupole interaction is dominated by the displacements in the first- and second-nearest-neighbor atoms.[9,11] This is in qualitative agreement with the fact that for $x > 0.02$ the ^{39}K NMR signal decreases in intensity below T_c and broadens without resolution into the two lines for $\vec{H}\perp\vec{c}$ and $\vec{H}\|\vec{c}$. It is also noted that experimentally one finds even the resonance line with $\vec{H}\|\vec{c}$ broadened by inhomogeneous quadrupole interactions below T_c. This could happen only if the local symmetry is not axial.

C. Rounding of the discontinuity in the order parameter at T_c

From the birefringence measurements it appears that the small discontinuity in the order parameter at T_c observed in pure $KMnF_3$ is present also in the mixed crystals with Rb concentrations of $x = 0.02$ and $x = 0.04$. For $x \geq 0.06$ the transition becomes continuous within the experimental resolution of our apparatus. Furthermore, there is some evidence that the rounding of the discontinuity occurs gradually and for the largest concentrations the birefringence goes to zero with almost zero slope.

It seems reasonable to ascribe the rounding of the transition to fluctuations of the Rb concentration within "correlation volumes."[15] In such a model one assumes that the transition occurs with a discontinuous jump in the order parameter within each individual "correlation volume." In pure $KMnF_3$ the "correlation volume" is practically

equal to the volume of the crystal itself while in the mixed crystals the correlation volume decreases rapidly with increasing Rb concentration. For small "correlation volumes" the statistical fluctuations in Rb concentration between different volumes then becomes appreciable and results in a distribution of transition temperatures. An estimate of the effect can be obtained by assuming a statistical model for the distribution of transition temperatures, which yields the expression

$$\Delta T_c \sim \frac{\partial T_c}{\partial x}\left(\frac{x}{N(x)}\right)^{1/2}, \tag{4.6}$$

where $N(x)$ is the number of Rb or K sites in a "correlation volume" and $|\partial T_c/\partial x| = 360$, as deduced from the experimental data shown in Fig. 7. In the $x = 2$- and 4-at.% samples the rounding is less than the instrumental resolution (~50 mK), whereas at $x = 6$-at.%, $\Delta T_c \sim 250$ mK and at $x = 15$-at.% it is as much as 2 °K. For $x = 0.06$ one obtains from (4.6) $N(0.06) \sim 1.3 \times 10^5$, which is indicative of a correlation distance $l \sim aN^{1/3} \sim 200$ Å or roughly 50 lattice spacings. For $x = 0.15$ one has $N(0.15)$ $\sim 5 \times 10^3$ corresponding to $l \simeq 17a$, which is at the limit for a meaningful definition of long-range order.

It should be noted that the definition of a unique transition temperature within a "correlation volume" does not imply that the order parameter is uniform within this volume. In fact from the NMR results we deduce that the variation of the rotation angle φ occurs on a distance of the order of the average distance between Rb impurities, which is about two lattice spacings for $x = 0.15$ while a "correlation volume" containing 10^4 sites corresponds to about twenty lattice parameters. We can rephrase this concept by saying that the rounding of the discontinuity at T_c represents an effect of macroscopic inhomogeneity while the broadening of the NMR line reflects a microscopic nonuniformity in the order parameter.

V. SUMMARY AND CONCLUSIONS

The crystal $KMnF_3$, with partial substitution of the K atoms with other cations, affords an excellent model system of structural phase transitions in disordered lattices. The utilization of both a macroscopic technique like birefringence and a microscopic technique like NMR has revealed itself very useful and has produced interesting and somewhat unexpected results, which are summarized below. The transition temperature was found to decrease upon substitution of K with Rb. In the

concentration range $x \le 0.10$ the dependence can be expressed approximately as $T_c(x) = T_c(0)(1 - 2x)$. Actually this law represents, for small Rb concentrations, a quadratic dependence of the transition temperature upon the concentration $(1 - x)$ of K atoms. It is hoped that the extension of the molecular-field-approximation treatment in terms of local coordinates will yield some indicative theoretical results to be compared with the experiments.

The transition loses the first-order discontinuous jump in the order parameter for a Rb concentration between 4 and 6 at.%. The rounding of the discontinuity can be explained in terms of a distribution of transition temperatures due to statistical fluctuations of concentration within "correlation volumes" which represent the limiting size over which the long-range order establishes at T_c. Below T_c the average rotation angle of the MnF_6 octahedra appears to remain the order parameter for the structural transition but its magnitude is rapidly reduced in the Rb substituted crystals with respect to pure $KMnF_3$. Within each domain the order parameter is nonuniform even over distances of a few lattice spacings. This situation is very reminiscent of the behavior of the local magnetization in disordered magnetic systems below T_c (or T_N) whereby the magnetic moment of the cell depends on whether the cell is occupied by a magnetic ion or a substituted diamagnetic one.

It is hoped that the present investigation will stimulate further theoretical and experimental studies of cooperative structural phenomena in disordered crystals. In particular, it would be interesting to extend the study of mixed crystals of $KMnF_3$ with K atoms substituted by Na and/or Cs atoms. According to the values of the Goldsmith ratio in Table I it would appear that the Na substitution should result in an increase of T_c while the Cs substitution could yield either an increase or a decrease of T_c.

[1]*Structural Phase Transitions and Soft Modes*, edited
by E. J. Samuelsen (Universitetsforlaget, Oslo, 1971).

[2]*Local Properties at Phase Transitions*, edited by K. A.
Müller and A. Rigamonti (North-Holland, Amsterdam,
1976).

[3]R. Blinc and B. Zeks, *Soft Modes in Ferroelectrics
and Antiferroelectrics* (North-Holland, Amsterdam,
1974).

[4]K. A. Müller, in Ref. 2.

[5]H. Thomas, in Ref. 1.

[6]V. J. Minkiewicz and G. Shirane, J. Phys. Soc. Jpn. 26,
647 (1969); G. Shirane, V. J. Minkiewicz, and A. Linz,
Solid State Commun. 8, 1941 (1970).

[7]G. Burns, Phys. Rev. B 13, 215 (1976), and references
therein.

[8]D. J. Benard and W. C. Walker, Rev. Sci. Instrum. 47,
122 (1975).

[9]F. Borsa, Phys. Rev. B 7, 913 (1973).

[10]A. Abragam, *The Principles of Nuclear Magnetism*
(Oxford U. P., Oxford, England, 1961).

[11]F. Borsa, in Ref. 2.

[12]H. D. Megaw, *Crystal Structures: A Working Approach* (Saunders, Philadelphia, Pa., 1973).

[13]B. Okai and J. Yoshimoto, J. Phys. Soc. Jpn. 39, 162
(1975).

[14]R. A. Tahir-Kheli, L. C. M. Miranda, and S. M.
Rezende, Nuovo Cimento B 30, 335 (1975), and references therein.

[15]The "correlation volume" introduced here should not
be confused with the correlation length describing the
onset of short-range order near a phase transition.
In fact the "correlation volume" is viewed here as a
macroscopic volume corresponding to the limit of infinite correlation length.